A new double layer super-capacitor made by free-standing activated carbon membranes and highly concentrated potassium acetate solutions

*M. Tribbia[a], N. Pianta[b], G. Brugnetti[b], R. Lorenzi[b], R. Ruffo[b]**

a Faculty of Production engineering, Energy storage and energy conversion systems, Bremen University, 28359, Bremen, Germany
b Department of Materials Science, University of Milano Bicocca, via R. Cozzi 55, I-20125 Milan, Italy

** Corresponding author: riccardo.ruffo@unimib.it*

Abstract

Water in salt solutions are a new class of electrolytes developed with the aim of enlarge the electrochemical stability of aqueous electrolyte without decreasing the transport properties. Among them, aqueous solutions of potassium acetate (CH_3COOK, AcK) have received little attention, despite its large solubility in water at room temperature (25 mol kg^{-1}) and the very low cost. With the idea of developing cost-effective and good performing Electrochemical Double Layer Capacitors (EDLC), a symmetric device based on a low-cost coal derived carbon (F400) and highly concentrated AcK solutions as electrodes and electrolytes, respectively was fabricated and optimized. The best results are obtained with the system F400/20 mol kg^{-1} AcK/F400 able to deliver a gravimetric energy density of 26 Wh kg^{-1} at an average power of 1.4 kW kg^{-1}.

Keywords

Potassium acetate, water in salt electrolyte, activated carbon, electrochemical double layer capacitor

1. Introduction

The growing demand for energy storage at various scales is making it clear that there is no single technology that can satisfy all different needs [1]. In high power and low energy applications, for example, electrochemical double layer capacitors (EDLCs) are commonly used. This class of supercapacitors usually adopts carbonaceous electrodes immersed in an electrolyte solution [2,3]. EDLCs are conceptually similar to classical dielectric capacitors regarding the charge storage mechanism and the use of symmetrical electrodes, however the presence of the electrolyte makes them electrochemical devices. An EDLC, indeed, accumulates ion amounts onto the electrode surface as a function of the applied voltage, while in a pseudo-capacitor (PC) the charge storage mechanism is also related to a surface-driven redox reaction. The main structural parameter for EDLC electrodes is the contact area between the electrode and the electrolyte: the larger the surface area, the greater the number of accumulated ions at the same voltage and therefore the larger will be the stored energy. For this reason, EDCLs use highly porous carbonaceous materials that have different functional heteroatomic groups in their structure. These materials are often treated at high temperatures, often with chemical agents, to further develop their porosity. Carbonaceous materials for EDLCs can be classified as nanostructured carbons (micro or nanotubes) [4] or active carbons (ACs) [3, 5-8]. Despite their excellent performances, nanostructured carbons are still expensive and difficult to prepare. In contrast, activated carbons are commonly used in commercial devices thanks to their economical price and easy preparation routes. ACs can be obtained as by-product in industrial processes [8] or by biomasses waste [9-10], making them examples of circular economy materials.

Given the capacitive nature of the charge accumulation mechanism, the electrochemical stability of the electrolyte plays a crucial role in supercapacitors because it limits the device performances. Commercial ECDLs use liquid electrolytes thanks to the high ionic conductivity, the availability, and the cost [6]. Liquid electrolytes can be classified in three families: aqueous electrolytes, organic electrolytes and ionic liquids. Water based

electrolytes, such as H_2SO_4, KOH, and NH_4Cl aqueous solutions, have several advantages over the other families thanks to the higher electrochemical mobilities of ions and the lower cost [5]. However, the small electrochemical stability window of water limits the operative voltage of the devices at 0.8-1.0 V, thereby affecting the stored energy. An alternative approach is the use of highly concentrated aqueous electrolytes, the so-called "water in salt", to change the activity coefficient of the water or to form a quasi-stable passivation layer at the electrode surface [11-12]. Literature examples of water in salt coupled with symmetric AC electrodes in EDLCs mainly report the use of LiTFSI with concentrations of 21 mol of salt per kg of solvent [13,14] or 31.3 mol kg^{-1} [15]. Depending on the inherent characteristic of AC electrodes and devices, these EDLC examples can deliver a gravimetric energy between 5.8 and 30.4 Wh kg^{-1} over potential ranges of 2.5 and 2.9 V [14-15]. Another case of EDLC using water in salt and AC electrodes is that reported by Tian et al. [11] using a 7.6 mol kg^{-1} CH_3COOK (AcK) solution. Although this concentration falls within the lower limit of the "water in salt" definition, it allows the increase of the voltage up to 2.0 V delivering a gravimetric energy of 19.8 Wh kg^{-1}. The latter example is important because AcK is much less expensive than LiTFSI and concentrations up to 25 mol kg^{-1} can be reached.

With the idea of developing a very economical energy storage device, a new EDLC configuration is presented here featuring two symmetrical, self-standing AC membranes separated by highly concentrated solutions of AcK in water. These electrodes are based on a low cost coal-derived carbon commonly used to produce purification filters. After the experimental details, the work is organized in the following structure: first, the physico-chemical characteristics of both the electrolytic solution and the carbon are presented, then the function characterization of symmetrical devices with high load self-standing electrodes is described. At the end, before the conclusions, a discussion on the concept of capacitance in these systems is reported, considering how to obtain the "effective" capacitance of ECDL or pseudo-capacitors from experimental charge/discharge measurements. All the electrochemical measurements are also performed in a 6 mol l^{-1} KOH solution for comparison purposes.

2. Experimental

2.1 Materials.

The coal-derived AC (F400) is produced by Chemviron™ and it is commonly used to fabricate purification filters. The material was kindly provided by Calgon Carbon® Italy s.r.l., Rho, Italy. This AC is activated through a steam-activation process and it is sold as a good adsorbent material for water filters. Even if it's a coal-derived carbon, it has already been inserted in a recycling process by Calgon Carbon® itself. The activation process, as indicated by Chemviron™, is a partially oxidizing process at 500°C followed by a pyrolysis step at 1000°C in inert atmosphere. No further chemical or thermal activation was performed before the use. Potassium acetate (98%) and potassium hydroxide (85%) were purchased from Alpha Aesar. Three solutions: 6 mol l^{-1} KOH (solution volume), 20 mol kg^{-1} (solvent mass) and 25 mol kg^{-1} CH_3COOK were prepared using Milli-Q water as a solvent. Each solution was deaerated under vacuum for 10 min followed by a nitrogen bubbling step for the removal of oxygen.

2.2 Material characterization.

A powder diffractometer Rigaku® Miniflex, equipped with a Cu source (1.54 Å), was used for XRP measurement. recording the diffractograms from 15 to 90 2θ deg with a step rate of 1 deg min^{-1} using a quartz sample holder. Raman measurements were carried out at room temperature by a confocal labRAM (Horiba Jobin-Yvon) spectrometer, operating in backscattering configuration with a focal layer thickness of few microns. A He-Ne laser line at 632.8 nm was used as exciting source with spectral resolution of about 2 cm^{-1}. The scattered light was detected by a charge coupled device (CCD-Sincerity, JobinYvon). A microscope (Olympus BX40) was used to focus the excitation on the samples and to collect the scattered radiation, by a Long Working Distance 50x objective with a numerical aperture of 0.60, with a resulting sampled area of 5 µm in diameter, and a laser power on the sample of <1 mW. A Zeiss® GeminiSEM 450 apparatus in a high-vacuum configuration has been used to obtain the SEM images. A field emission source has been used as electron source and the electrons have been accelerated using an electric potential around 5-10kV. The electrical and electrochemical characterization of the AcK solutions was performed by Impedance Spectroscopy (IS) and cyclic voltammetry (CV), respectively, on solutions purged with N_2 to remove the dissolved O_2. A conductivity cell with Pt electrodes was used for IS

measurements. The amplitude voltage stimulus was 10 mV and the explored frequency range was between 1 and 50 kHz. The solution resistance (R_{el}) was calculated from the high frequency intercept ($-Z_{im}=0$, $Z_{real}=R_{el}$) of the corresponding Nyquist plot. CV curves were measured in a three-electrode flooded cell at scan rate of 1 mV s^{-1} using a well-polished glassy carbon, a Pt mesh and a Saturated Calomelan Electrode (SCE) as working, counter, and reference electrodes, respectively.

2.3 Electrode preparation.

Self-standing high-load electrodes were prepared by an unconventional route mixing the active material with conductive carbon and an organic binder in the weight ratio 8:1:1. First, F400 was blended and grounded together with SuperP conductive carbon in a mortar. Then, a suspension of PTFE in water (Sigma-Aldrich, 60%wt) was added to the powder and mixed to obtain a homogenous dough, which was then pressed in a calender at different thicknesses several times to obtain a flexible film of 180 μm in thickness. The residual water was eliminated by drying the film at 80°C under vacuum overnight. The electrodes were cut in a disc-shape having a diameter of 1.6 cm. With this procedure, active-mass loads of 12 mg cm^{-2} (670 mg cm^{-3}) were typically achieved.

2.4 Electrochemical characterization of devices.

The electrochemical measurements on the devices were performed using a sealed, Swagelok-type, two electrode cells in symmetric configuration (F400/electrolyte/F400). The cells were assembled with N_2-purged electrolyte in dry environment to avoid the presence of molecular oxygen in the solutions. Galvanostatic cycling with potential acceleration (GCPL) at different gravimetric currents were carried out at 25°C in an environmental chamber (Angelantoni ACS), using a Bio-Logic VSP-300 galvanostat-potentiostat. Rate tests were performed using the following protocol: 25 cycles at 0.1 A g^{-1}, then the current is increased every 25 cycles to 0.2, 0.5, 1.0, and 2.0 A g^{-1}, and finally reduced again to 0.1 A g^{-1}. The total number of cycles in this test is thus 150. Long cycling experiments (10^4 cycles) were conducted at 1.0 A g^{-1}.

3. Results and discussion

3.1 Characterization of CH_3COOK-based electrolytes.

The complete physico-chemical investigation of highly concentrated potassium acetate solutions is outside the aim of the present paper, however, thanks to our studies (not yet reported), the concentrations of 20 and 25 mol kg^{-1} are promising thanks to their large cathodic stability and the good transport properties. In Figure 1a, the specific conductivities of the two solutions are reported in an Arrhenius graph between 5 and 70°C. Both solutions show a behavior in accordance with the empirical VTF (Vogel Tamman Fulcher) model, valid for ionic conductors whose free volume depends on temperature. The specific conductivities of the 20 and 25 mol kg^{-1} are 55.6 and 31.0 mS cm^{-1}, respectively, at 25°C. According to literature data, the specific conductivity of a 6 mol l^{-1} KOH solution is 625 mS cm^{-1} [16]. In Figure 1b, the CV current/potential profiles are reported in the potential range between +1.50 and –1.50 vs. SCE. Using a current threshold of 0.1 mA cm^{-2} for the onset of the decomposition processes, the cathodic limits for the 20 and 25 mol kg^{-1} solutions are -1.3 and -1.4 V, respectively, Considering also the anodic limits, the stabilities of the solutions are around 2.5/2.7 V, which, however, should be carefully adjusted considering the application.

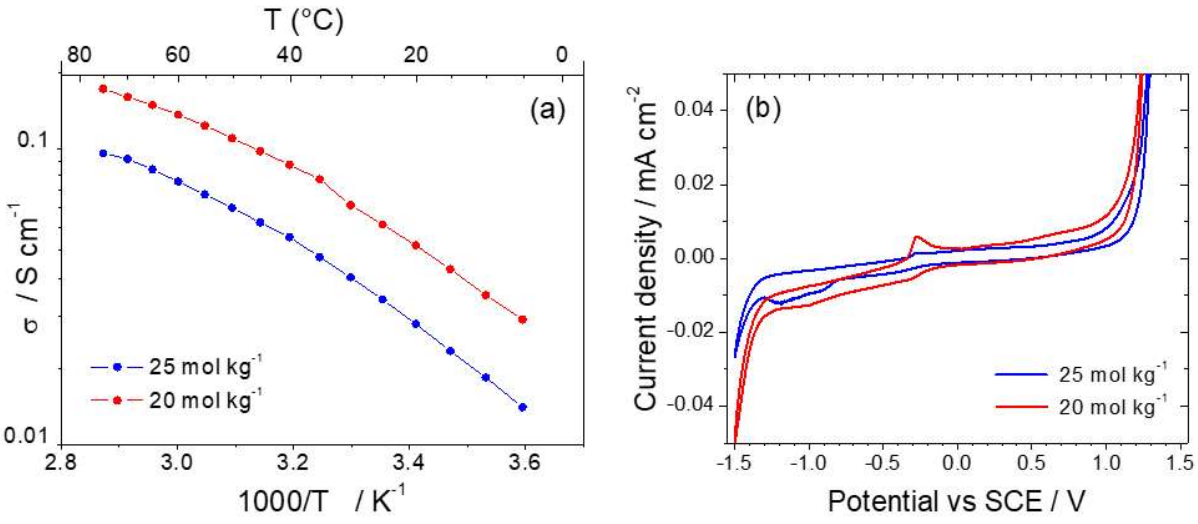

Figure 1. Arrhenius plot (a), and CV profiles on gold electrode at 1 mV s^{-1} (b) of the 20 and 25 m AcK solutions.

The redox process at around -0.2 V s attributed to the insoluble products formed onto the electrode surface at very high and very low potentials.

3.2 Carbon characterization.

The chemical and morphological characterization of F400 is reported in Figure 2. SEM images are obtained at different magnifications to reveal the presence of secondary structures and to obtain the primary particle size. Secondary structures of several microns in size are visible in the low magnification image (Figure 2a) and are made up by porous agglomerates of smaller grains having dimensions of tens of nm (Figure 2b). The porous structure of the secondary particles is confirmed in the BET analysis (Figure 2d), the F400 AC has a surface area of 1066 m^2 g^{-1} and an average pore size dimension of 5.6 nm, which classifies this carbon as a mesoporous structure. The CHNS chemical analysis reveals the purity of the sample, consisting of 94% of carbon (Figure 2c). Sulfur impurities coming from the coal remain in the sample, while a relative low amount of oxygen is incorporated during the thermal treatments. This result agrees with the absence of a additional chemical activation step.

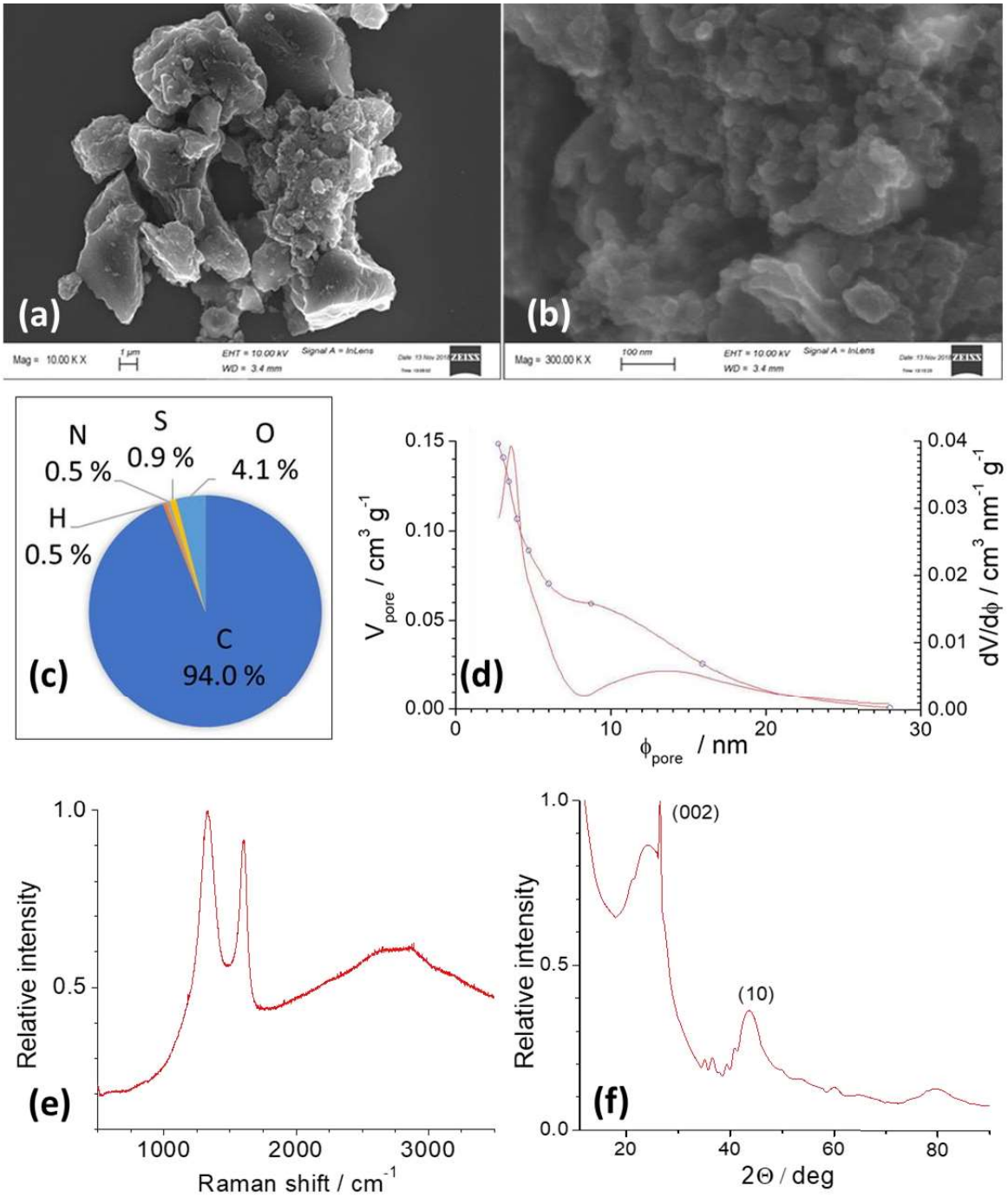

Figure 2. Morphological, chemical and physical characterization of F400: (a) and (b): lower and higher magnification SEM images, (c) CHNS results, (d) BET analysis, (e) Raman analysis, (f) XRD analysis.

The structural features of F400 are investigated by both Raman spectroscopy and XRP analysis (Figure 2). The Raman spectrum is dominated by the presence of the G and D bands at 1600 and 1325 cm^{-1}, respectively, plus a

large bell-shaped peak relative to the second order region (Figure 2e). The G band is characteristic of the crystalline periodic arrangement of graphite, while the presence of the D band is due to both finite size effect (nanometric graphite) and/or the presence of structural defects that break the transitional symmetry of graphite. The D/G intensity ratio is used to quantify defects in the carbon. In high purity, micrometric graphite the D/G ratio is 0.01, while in the case of F400 the value is 1.22, highlighting the presence of numerous structural defects. Furthemore, the position of the G band (1580 cm^{-1} in pure graphite) is shifted at higher wavenumbers (+20 cm^{-1}) in F400, an aspect that is probably related with the non-negligible presence of oxygen at the surface. The diffractogram of F400 (Figure 2f) also reflects the highly disordered structure of the carbon. The region between 20 and 30 in 2θ is characterized by the presence of a large peak corresponding to the wide distribution of the interlayer spacing along the c axis. A low intensity spike (002 graphite, SG $P6_3/mmc$) is also observed. The large reflection between 40 and 50 deg is attributed to the (10) peak, the convolution of the contributes from the basal (100, 101) and stack planes (101) in disordered turbostratic carbons.

3.3 Electrochemical characterization of the F400 symmetric EDLCs

F400 self-standing electrodes with high load (about 12 mg cm^{-2}) are used to fabricate three different ECDL devices using the symmetric AC/electrolyte/AC configuration and different aqueous solutions, i.e. 20 mol kg^{-1} AcK, 25 mol kg^{-1} AcK, and 6 mol l^{-1} KOH. The peculiar self-standing configuration of the electrodes has two main advantages over the use of current collectors: it reduces the amount of inert component of the cell, and avoids problems related to the current collector corrosion, in particular for the case of the AcK solutions. Polarization tests on bare Ni foam, for example, showed a corrosion current of $3x10^{-4}$ mA cm^{-2} at the corrosion potential of -0.485 V vs. SCE for the 25 mol kg^{-1} AcK solution.

Galvanostatic charge/discharge measurements are performed at different gravimetric currents, from 0.1 A g^{-1} to up to 2.0 A g^{-1}. Considering the electrode load and surface, these values correspond to current densities from 1.25 to 25.0 mA cm^{-2}. The explored potential range is from 0 to 1 V in the case of KOH and from 0 to 2 V for the AcK solutions; this latter value was selected to take advantage of the larger electrolyte potential window.

The charge/discharge profiles at different gravimetric currents are reported in Figure 3a for the different devices (from the lower panel to the upper one) and currents (different curves in the same panel, the last cycle is considered). The behavior in KOH is similar to that of an ideal ECDL, while significant deviations are observed in AcK, where a pseudo-capacitor contribute probably cannot be excluded. The device/electrode capacitance as well as the nature of the interaction will be discussed in depth in another paragraph. Here the performances of the devices in terms of specific capacity (Figure 3b), charge efficiency (Figure 3b), gravimetric energy density (Figure 4a) and average power density (Figure 4b) are analyzed. All devices need several cycles (15 to 20) at low current to stabilize performance, probably due to the large thickness of the electrode: cycle after cycle, more active material is involved in the electrochemical process until saturation [17].

At the end of the rate test (cycle 125/150), stable capacity values are observed in full agreement with those at cycle 20/25. At the lowest current, devices fed with 6 mol l^{-1} KOH, 20 mol kg^{-1} AcK, and 25 mol kg^{-1} AcK can deliver a discharge capacity of 24, 64, and 54 mAh g^{-1}, respectively. As the current increases the specific capacity decreases for all the devices, however at the highest rate (2.0 A g^{-1}) they still deliver 6, 24, and 20 mAh g^{-1}, respectively. Charge efficiencies increase with the rate, as expected in a capacitor where the self-discharge phenomena play an important role [18]. In fact, the greater is the current, the shorter is the time required for self-discharge to occur. At the highest rate, all the efficiencies approach 99.9%.

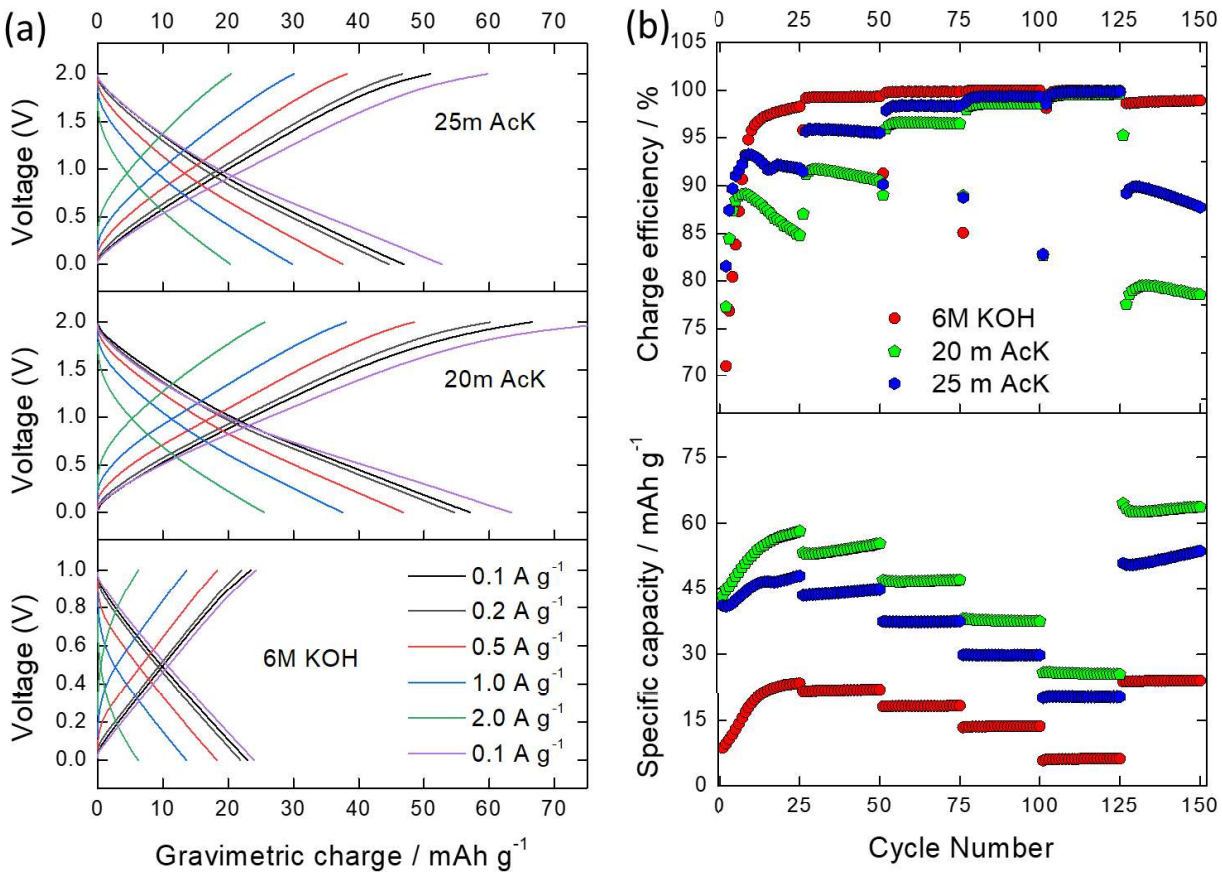

Figure 3. Charge/discharge profiles at different currents for the three devices (a); specific discharge capacity and efficiency vs. cycle number (b).

The corresponding gravimetric energy densities are obtained from the direct integration of the discharge curves of Figure 4a, while the gravimetric power densities are calculated as the average value of the energy over the delivering time. The best performance is obtained with the device fed with the 20 mol kg^{-1} AcK solution, capable of delivering 48, 44, 36, 26, and 15 Wh kg^{-1} at average powers of 0.15, 0.32, 0.77, 1.40, and 2.40 kW kg^{-1}, respectively. The KOH device is limited by the reduced potential range, decreasing both the specific capacity and energy, while the performance of the 25 mol kg^{-1} AcK electrolyte is affected by the low conductivity of the solution.

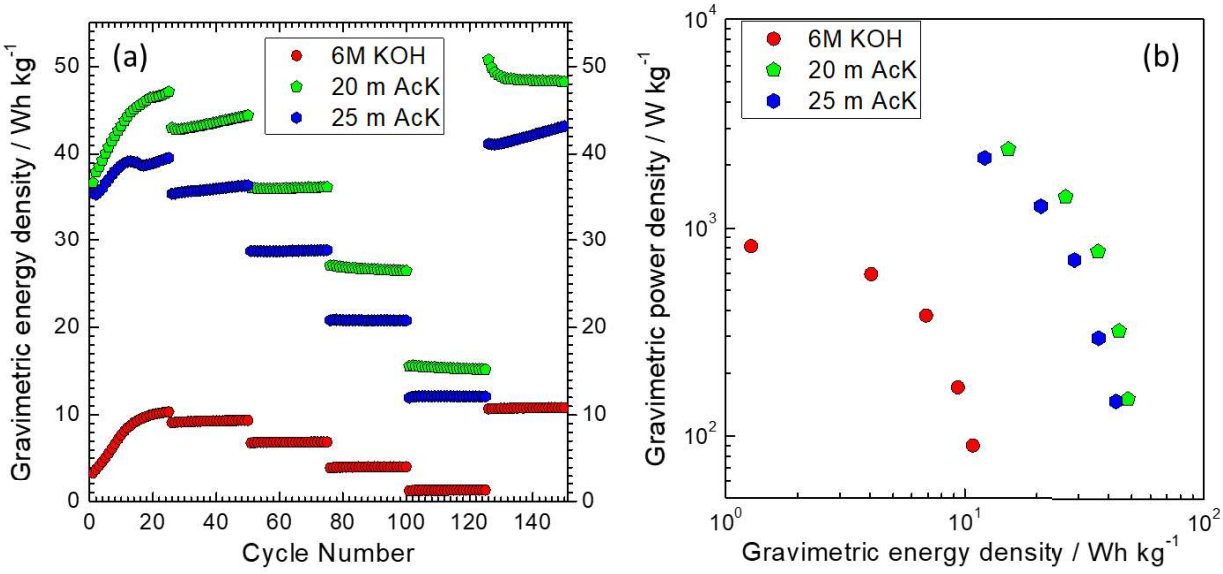

Figure 4. Gravimetric energy density during discharge at different currents (a) and Ragone plot (b) for the three devices (a).

3.4 Long term stabilities and cut off effect

At the end of the rate test, the 20 mol kg^{-1} AcK and the 6 mol l^{-1} KOH devices are charged and discharged for $1x10^4$ cycles at 1 A g^{-1} (Figure 5). The device fed with the alkaline electrolyte shows very good stability over the whole cycling, with 95% and 91% of capacity and energy retention, respectively, with a charge efficiency > 99.9 %. On the contrary, the device made using the water in salt solution shows an increment in the performances up to 1300 cycles, then both the specific capacity and energy decrease with the number of cycles and at the end the capacity and energy retentions are 80 and 72% of the maximum values. The difference between the two retentions suggests that the degradation is not just related to the charge storage ability, but also to the increase of resistive components in the device which increase the overpotentials, further reducing the energy compared to the charge. The charge efficiency also reflects the partial irreversibility of the process, being about 99.0% along the measurement.

To optimize the device cyclability in AcK, the effect of the cut-off potential on the performances in the range 1.0-2.0 V is also studied. The results, reported in Figure 6, show the trade-off between the stored charge and the reversibility: by moving the cut-off from 1.6 V to 2.0 V, the specific capacity increases from 22 to 32 mAh g^{-1}, while the efficiency drops from 99.7 to 98.7 %. The lower efficiency is probably due not only to the system self-discharge, but also to a partial irreversible reaction with the electrolyte, as discussed in the next section. For this reason, a fresh device is pretreated at 0.1 A g^{-1} for 25 cycles and then cycled $1x10^4$ times at 1 A g^{-1} between 0 and 1.6 V. In this condition, the F400/20 mol kg^{-1} AcK/F400 system shows good specific capacity, good gravimetric energy density, at least double of that of KOH, and 100% retention for both capacity and energy (see blue curve in Figure 5).

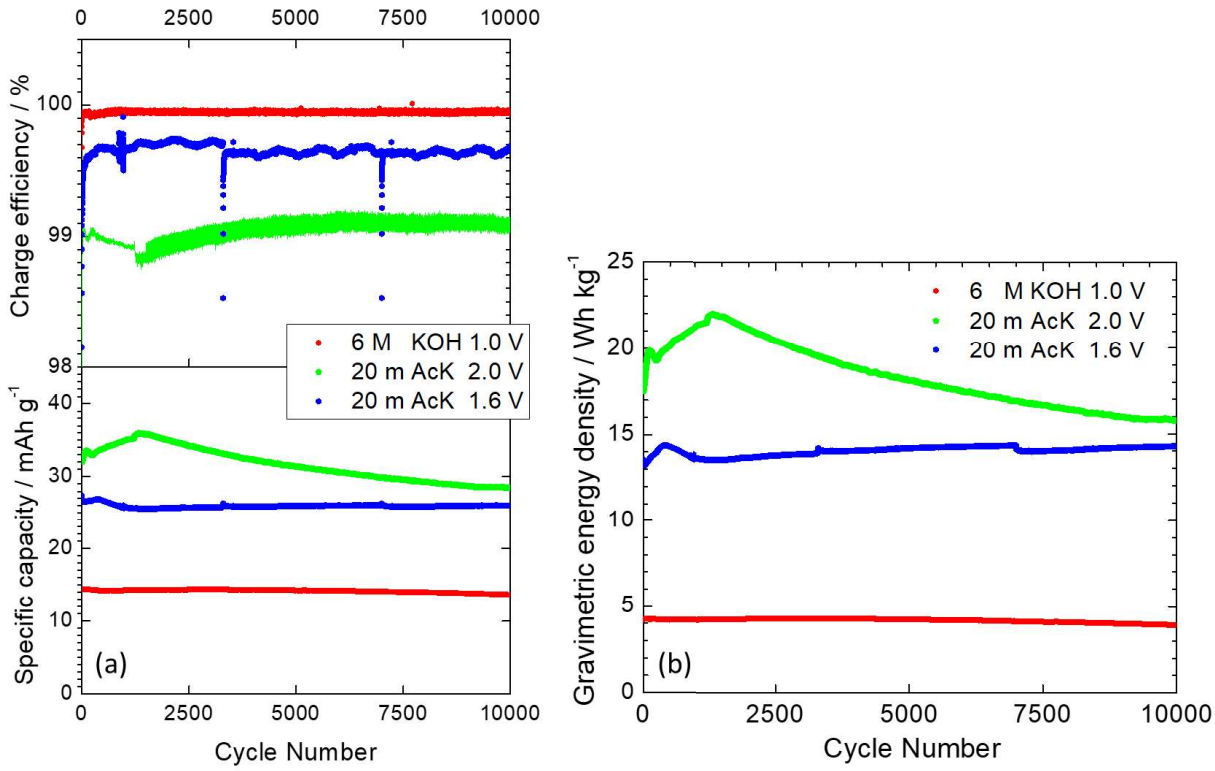

Figure 5. Specific capacity (a, lower panel), charge efficiency (a, upper panel) and gravimetric energy density during 10^4 cycle at 1 mA g^{-1} for the F400/6 M KOH/F400 (red points) and for the F400/20 m AcK/F400 device cycled between 0.0 and 2.0 V (green points) and between 0 and 1.6 V (blue points).

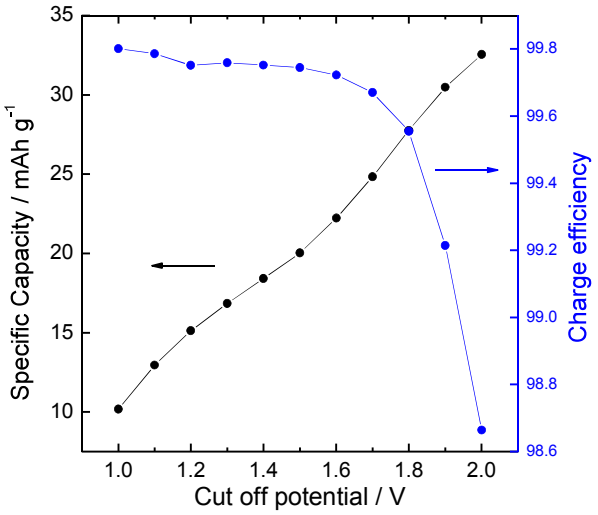

Figure 6. Specific capacity (left axis, black) and charge efficiency (right axis, blue) for the F400/20 m AcK/F400 device cycled using different cut off voltages.

3.5 The "effective" capacitance of the system and the nature of charge accumulation

In discussing the performance of EDLCs or pseudocapacitors, the specific capacitance (C_S, F g^{-1}) is often used as a qualitative and quantitative parameter. Being the ratio between the amount of stored charge and the explored voltage window of pure capacitor, the specific capacitance is often calculated from experimental data without considering that many systems are far from ideal and even small deviations from ideality lead to erroneous energy values. Indeed, the energy is often obtained from the capacitance using the relationship:

$$E = \frac{1}{2} C \Delta V^2 \qquad \text{(eq. 1)}$$

where ΔV is the explored voltage window. Again, this relationship is valid only for ideal systems and small deviations from ideality lead to huge differences in energy, not only because the capacitance itself, but also for the wrong potential value (ΔV). Few years ago, Yang & Mai published a seminal work underlined these considerations [19]; their point of view is discussed below and a more rigorous definition is given as well as a way to calculate the "effective" capacitance (C_{eff}) of a device or material.

Regardless of the charge/discharge conditions, the energy introduced or delivered by a device is the integral of the power over the time, which is given by the voltage multiplied by the current:

$$E = \int P(t)dt = \int_{t=0}^{t=f} V(t)i(t)dt = \int_0^Q V(q)dq \qquad \text{(eq.) 2}$$

where $q = i(t)dt$ is the charge at the time t and Q is the capacity of the device. Therefore, apart from the experimental condition of applying a constant voltage, in which the direct $i(t)dt$ integration should be performed, the energy can be obtained from the integration of charge/discharge curves (V vs. q).

In a pure capacitor, such as a dielectric capacitor, the relationship between V and q is a straight-line across all the ΔV within the window stability (V should be less than the breakdown value), and since the slope is the inverse of the capacitance (C=ΔQ/ΔV), the eq. 2 collapses in eq.1. In non-ideal systems, such as all the pseudo-capacitors and several EDLCs, the V(q) curve is not a straight-line, and the energy must be obtained directly from eq. 2 for two main reasons: the capacitance depends on the voltage, and the presence of overpotentials, including the iR drop, alters the ΔV value. This latter aspect is often underestimated: however, the system works longer at higher voltage during charge and more time at lower voltage during discharge.

The measurement of the V(q) profiles makes the determination of the specific capacitance useless, however Yang and Mai have proposed that these two values (C_{eff} and ΔV) can be deduced backwards from the energy "because people would prefer to directly use specific capacitance and capacitance to evaluate electrochemical performance of materials and devices" [19]. However, having two variables (C and ΔV) and one equation (eq. 1), the proposed method is arbitrary since it uses the total explored range (ΔV_{max}) or half of it ($0.5\Delta V_{max}$) to obtain the "effective" specific capacitance from gravimetric energy density. Furthemore, this approach does not consider the different effect of overvoltages between charge and discharge cycles.

Even in systems similar to ideal capacitors, such as EDLCs, a more complex analysis should be performed, at least to validate the method. By deriving the charge/voltage profiles of the galvanostatic measurements, one can get an idea on the dependence of the capacitance on voltage. In Figure 7a, the charge (solid) and discharge (dashed)

curves of our device in KOH are shown at current of 0.2 A g^{-1}. The integrals of these curves give the gravimetric energy densities of charge/discharge (12.3 and 9.4 Wh kg^{-1}, respectively). The derivatives of the gravimetric charges vs. the voltage are reported in Figure 7b: they show a good overlap between charge and discharge and can be divided into three zones: in the initial phase the resistive elements dominate the slope (resistance losses), then there is a region where the derivative is voltage independent and finally, close to the cut-off voltage, the derivative changes again in presence of Faradaic charge contributes (irreversible in this case). Therefore, the "effective" capacitance of the system (C_{eff}) should be extrapolated from the curve where the C is independent on the voltage.

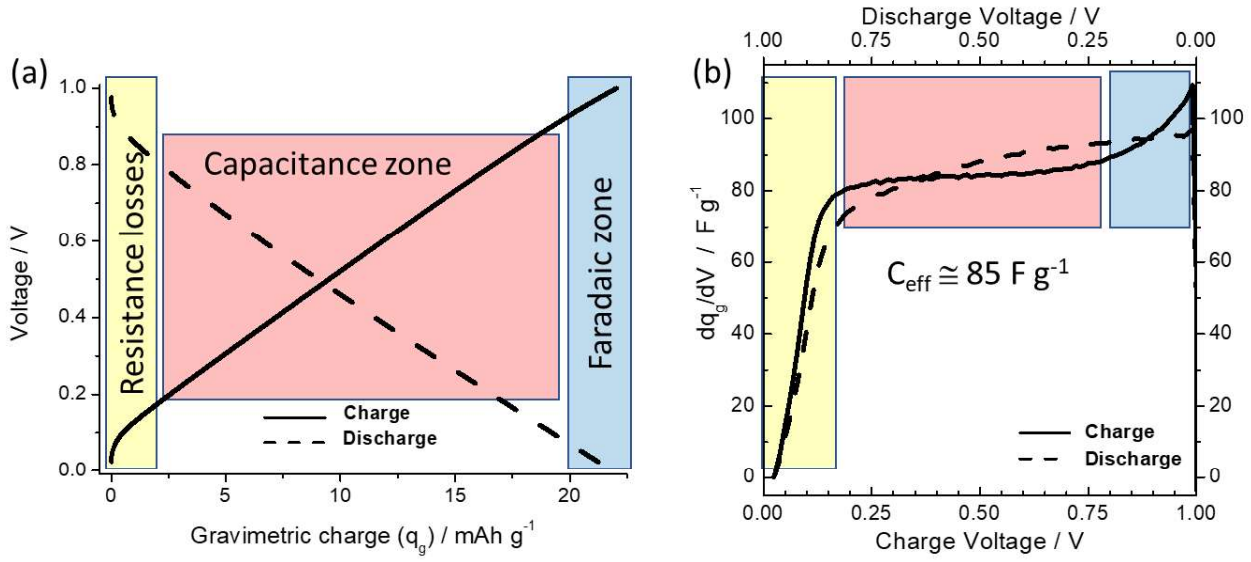

Figure 7. (a) Charge/discharge profile of the F400/6M KOH/F400 device at 0.2 A g^{-1} between 0.0 and 1.0 V, and (b) corresponding differential charge vs. voltage during charge (lower X axis) and discharge (upper X axis)

Using the derivative curves, one can estimate C_{eff} in the central zone (about 85 F g^{-1} in Figure 7b), and therefore the "experimental" ΔVs in eq. 1 can be calculated backwards, which in this case gives 0.55 V for the charge and 0.45 V for the discharge. These values are nearly half of the explored range, the use of $0.5\Delta V_{max}$ seems reasonable. However, this latter procedure of using *always* using $0.5\Delta V_{max}$, has two disadvantages: it does not discriminate between charging and discharging processes, since the capacitance should be the same while the

ΔV could be different and, more important, is strongly dependent on the applied current. Figure 8a shows the derivative of the gravimetric charge at different current densities for both the investigated systems (6 mol l^{-1} KOH and 20 mol kg^{-1} AcK). Even in a quasi-ideal ECDL such as the AC/KOH/AC device (see the profiles in Figure 3a), the capacitance depends on the voltage at low and high currents. In fact, at low current values, the Faradaic contributes affect the charging behavior near to the cut-off regions since irreversible reactions have more time to develop; while at very high current the resistive terms take the control of the kinetic and the capacitance is never constant. In any case, C_{eff} is almost independent on the current density, as expected, while the ΔV is significantly reduced at high current (about 0.25V at 1 A g^{-1}). So, again, it should be better to estimate C_{eff} from the measurements and then calculate ΔV.

The case of the highly concentrated electrolyte is much more complicated (Figure 8b), due to the wider potential range and the peculiar interactions between the electrode/electrolyte components. In the low potential region, the reduced ionic conductivity of the system affects the behavior more effectively than the KOH, then the intermediate, capacitive zone is observed. Here, the C_{eff} can still be estimated, it is more current dependent than in the KOH case, but at 0.2 A g^{-1} the values in the two electrolytes are in good agreement, 100 vs. 85 F g^{-1}, respectively. Hence, this value appears to be related more to the electrode itself than to the electrolyte. At high voltage, during charge (V>1.5), the derivative increases due to the Faradaic contributes which are more reversible than to KOH. In fact, a belly shaped peak is observed in this potential region during discharge (dashed lines) probably due to the dismantling of the Faradaic interphase. The presence of this belly shaped peak in the discharge can be considered as indicative of the presence of pseudo-capacitor behavior.

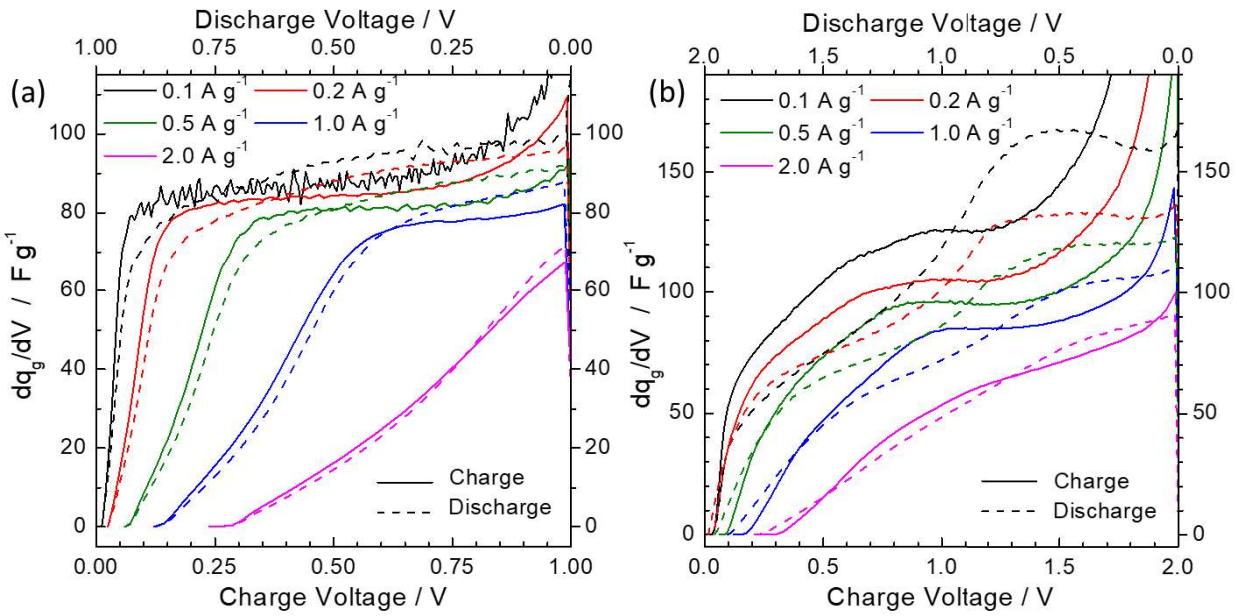

Figure 8. Differential charge vs. voltage during charge (lower X axis) and discharge (upper X axis) at different gravimetric currents for the F400/6 M KOH/F400 device (a) and the F400/20 m AcK/F400 (b) devices.

In conclusion, the energy of an EDLC device should be measured directly using Eq. 2 which gives the real value without misunderstandings. If one wants to report the specific capacitance of an EDLC, the charge/discharge curves and the corresponding q/V derivatives should be carefully analyzed in order to discriminate among different kinetic regimes.

4. Conclusions

The possibility of using AcK-based water in salt solutions has been demonstrated in ECDL capacitors by analyzing the critical aspects in terms of salt concentration and operative parameters of the device. As active materials, a well available and cheap coal derived carbon was used, the electrode layers were formulated as high load self-standing membranes with no current collectors. The performance of the devices was evaluated in terms of specific capacity (mAh g^{-1}) and gravimetric energy density (Wh kg^{-1}), while the device specific capacitance (F g^{-1}) was discussed by analyzing the differential capacity curves. The best results were obtained using the F400/20

mol kg^{-1} AcK/F400 device capable of delivering 26 Wh kg^{-1} at 1.4 kW kg^{-1}, energy retention is 72% after 10^4 cycles. When the cut-off voltage is reduced from 2.0 to 1.6 V, the performance decreases to 14 Wh kg^{-1} at 1.1 kW kg^{-1} with an efficiency > 99.6% and no degradation up to 10000 cycles. For comparison, the F400/KOH/F400 device cycled in the 0-1 voltage range showed 4 Wh kg^{-1} at 0.6 kW kg^{-1}.

Acknowledgements

This work has been financed by: Ministry of University and Research (MIUR) through grant "Dipartimenti di Eccellenza - 2017 "Materials For Energy",

References

[1] P. Gardner, F. Jones, M. Rowe, A. Nouri, H. van de Vegte, V. Breisig, C. Linden, T. Pütz, WORLD ENERGY COUNCIL World Energy Resources, (2016). https://www.worldenergy.org/wp-content/uploads/2016/03/Resources-E-storage-report-2016.02.04.pdf.

[2] B.E. Conway, Transition from "supercapacitor" to "battery" behavior in electrochemical energy storage, Proc. Int. Power Sources Symp. (1991) 319–327. https://doi.org/10.1109/ipss.1990.145856.

[3] P. Simon, Y. Gogotsi, P. Simon, Y. Gogotsi, N. Materials, Materials for electrochemical capacitors, 7 (2019) 845–854.

[4] C. Cao, Y. Zhou, S. Ubnoske, J. Zang, Y. Cao, P. Henry, C.B. Parker, J.T. Glass, Highly Stretchable Supercapacitors via Crumpled Vertically Aligned Carbon Nanotube Forests, Adv. Energy Mater. 1900618 (2019) 1–11. https://doi.org/10.1002/aenm.201900618.

[5] G. Wang, L. Zhang, J. Zhang, A review of electrode materials for electrochemical supercapacitors, Chem. Soc. Rev. 41 (2012) 797–828. https://doi.org/10.1039/c1cs15060j.

[6] F. Wang, X. Wu, X. Yuan, Z. Liu, Y. Zhang, L. Fu, Y. Zhu, Q. Zhou, Y. Wu, W. Huang, Latest advances in supercapacitors: From new electrode materials to novel device designs, Chem. Soc. Rev. 46 (2017) 6816–6854. https://doi.org/10.1039/c7cs00205j.

[7] E. Frackowiak, Carbon materials for supercapacitor application, Phys. Chem. Chem. Phys. 9 (2007) 1774–1785. https://doi.org/10.1039/b618139m.

[8] J. Huang, W. Xing, F. Subhan, X. Gao, P. Bai, Z. Liu, Y. Wang, Q. Xue, Z. Yan, Functionalization of petroleum coke-based mesoporous carbon for synergistically enhanced capacitive performance, J. Mater. Res. 32 (2017) 1248–1257. https://doi.org/10.1557/jmr.2017.36.

[9] H. Lu, X.S. Zhao, Biomass-derived carbon electrode materials for supercapacitors, Sustain. Energy Fuels. 1 (2017) 1265–1281. https://doi.org/10.1039/C7SE00099E.

[10] A. Jain, R. Balasubramanian, M.P. Srinivasan, Hydrothermal conversion of biomass waste to activated carbon with high porosity: A review, Chem. Eng. J. 283 (2016) 789–805.

https://doi.org/10.1016/j.cej.2015.08.014.

[11] Z. Tian, W. Deng, X. Wang, C. Liu, C. Li, J. Chen, M. Xue, R. Li, F. Pan, Superconcentrated aqueous electrolyte to enhance energy density for advanced supercapacitors, Funct. Mater. Lett. 10 (2017) 1750081. https://doi.org/10.1142/S1793604717500813.

[12] X. Zang, C. Shen, M. Sanghadasa, L. Lin, High-Voltage Supercapacitors Based on Aqueous Electrolytes, ChemElectroChem. 6 (2019) 976–988. https://doi.org/10.1002/celc.201801225.

[13] N. Kumar Thangavel, K. Mahankali, Y. Ding, L. Arava, Water-in-Salt Electrolytes for High-Voltage Supercapacitors. Meeting Abstracts; 2018, The Electrochemical Society; 2018. p. 148–148. https://doi.org/10.1149/MA2018-01/1/148

[14] K. Mahankali, N.K. Thangavel, Y. Ding, S.K. Putatunda, L.M.R. Arava, Interfacial behavior of water-in-salt electrolytes at porous electrodes and its effect on supercapacitor performance, Electrochim. Acta. 326 (2019) 134989. https://doi.org/10.1016/j.electacta.2019.134989.

[15] P. Lannelongue, R. Bouchal, E. Mourad, C. Bodin, M. Olarte, S. le Vot, F. Favier, O. Fontaine, "Water-in-Salt" for Supercapacitors: A Compromise between Voltage, Power Density, Energy Density and Stability, J. Electrochem. Soc. 165 (2018) A657–A663. https://doi.org/10.1149/2.0951803jes.

[16] R.J. Gilliam, J.W. Graydon, D.W. Kirk, S.J. Thorpe, A review of specific conductivities of potassium hydroxide solutions for various concentrations and temperatures, Int. J. Hydrogen Energy. 32 (2007) 359–364. https://doi.org/10.1016/j.ijhydene.2006.10.062.

[17] Aboutalebi, S. H., Chidembo, A. T., Salari, M., Konstantinov, K., Wexler, D., Kun Liu, H., & Xue Dou, S., Comparison of GO, GO/MWCNTs composite and MWCNTs as potential electrode materials for supercapacitors, Energy and Environmental Science 4 (2011) 1855–1865. https://doi.org/10.1039/c1ee01039e

[18] A. Lewandowski, P. Jakobczyk, M. Galinski, M. Biegun, Self-discharge of electrochemical double layer capacitors, Phys. Chem. Chem. Phys. 15 (2013) 8692–8699. https://doi.org/10.1039/c3cp44612c.

[19] P. Yang, W. Mai, Flexible solid-state electrochemical supercapacitors, Nano Energy. 8 (2014) 274–290. https://doi.org/10.1016/j.nanoen.2014.05.022.